Chemical Science

Accepted Manuscript

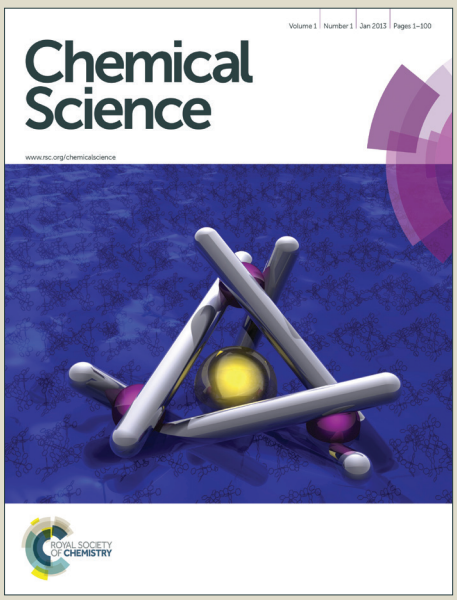

ROYAL SOCIETY OF CHEMISTRY

www.rsc.org/chemicalscience

Cite this: DOI: 10.1039/c0xx00000x

www.rsc.org/xxxxxx

EDGE ARTICLE

Self-assembly of a mesoporous ZnS/mediating interface/CdS heterostructure with enhanced visible-light hydrogen-production activity and excellent stability

Kui Li,[‡a] Rong Chen,[‡a] Shun-Li Li,[a] Min Han,[a] Shuai-Lei Xie,[a] Jian-Chun Bao,*[a] Zhi-Hui Dai[a] and Ya-Qian Lan*[ab]

Received (in XXX, XXX) Xth XXXXXXXXX 20XX, Accepted Xth XXXXXXXXX 20XX
DOI: 10.1039/b000000x

We designed and successfully fabricated a ZnS/CdS 3D mesoporous heterostructure with a mediating $Zn_{1-x}Cd_xS$ interface that serves as a charge carrier transport channel for the first time. The H_2-production rate and stability of the heterostructure involving two sulfides are dramatically and simultaneously improved by the careful modification of the interface state via a simple post-annealing method. The sample prepared with the optimal parameters exhibits an excellent H_2-production rate of 106.5 mmol/h/g under visible light, which is 152 and 966 times higher than that of CdS prepared using ethylenediamine and deionized water as the solvents, respectively, corresponding to the highest value among the CdS-based photocatalysts. Moreover, this heterostructure shows excellent photocatalytic stability over 60 h.

Introduction

Directly transforming solar energy into clean and renewable hydrogen via water splitting using suitable photocatalysts is especially important for resolving the ever-increasing energy crisis. Various nanomaterials,[1] particularly semiconductors,[2] have been investigated as photocatalytic hydrogen-evolution catalysts since TiO_2 was first reported to split water into hydrogen.[3] Metal sulfide semiconductor exhibits a suitable bandgap (Eg) that corresponds to visible light (approximately 44 % of solar energy);[4] it also exhibits excellent photocatalytic activity.[2c, 5] Among these sulfide semiconductors, CdS has been extensively investigated for hydrogen production because of its suitable Eg of approximately 2.4 eV and very negative conduction band (CB).[2a, 5d, 6] However, the fatal drawbacks of CdS, which include (i) a low H_2-evolution rate and (ii) a very limited lifetime arising from the rapid recombination of photo-excited charge carriers and the oxidization of CdS, respectively,[5d, 6a] restrict its practical application. As an effective solution to the low H_2-evolution activity, constructing CdS-based heterojunctions, such as TiO_2/CdS, ZnO/CdS, g-C_3N_4/CdS and ZnS/CdS,[5d, 7] has become a widely adopted strategy for improving the spatial separation of photo-generated electron/hole pairs. Nevertheless, the interface of the semiconductor heterojunction, which is an important factor that affects photocatalytic activity, is rarely investigated. Modulation of the matching of the lattice constant and the band structure in heterojunctions is difficult because of the limited number of candidate semiconductors with an appropriate intrinsic lattice constant and band structure.[8] Consequently, the semiconductor heterojunction may result in problems involving large lattice stress, high defect concentration and poor band-structure matching, which may inhibit the improvement of photocatalytic activity.[9] Inserting a conductive layer (such as Pt) that serves as a transport channel can dramatically improve the interface conductivity.[5b, 8, 10] However, the complicated process, poor ability to mediate the interfacial state, and the high cost of noble metals restrict its application.

With respect to the limited photocatalytic stability of CdS, passivation layers and surface modifications have been adopted to protect it from oxidation.[7a, 11] However, both of these methods can increase the lifetime of CdS at the cost of deteriorating its H_2-production rate because of the inhibition of photocatalytic reactions by the passivation layer and by the contaminated heterostructure.[5d, 7a] Indeed, the low H_2-production activity and limited photocatalytic stability primarily result from the poor separation and transportation efficiency of charge carriers. If we can embed a modulating interface with a tunable lattice constant as well as band structure, and enhanced interface state between a semiconductor heterostructure to modify the charge separation and transportation time and efficiency,[12] the H_2-evolution rate and photocatalytic stability may be effectively improved simultaneously.[5d, 13] Therefore, developing a semiconductor heterostructure with high photocatalytic activity and stability via carefully mediating the interface state is a subject of special importance from both scientific and practical perspectives.

In view of the aforementioned ideas, a ZnS/CdS porous heterostructure with a mediating interfacial layer acting as a transport channel (Scheme 1a) has been prepared using cation exchange[14] and post-annealing methods on the basis of the following points: i) ZnS/CdS exhibits quasi-type II characteristics and efficient photocatalytic hydrogen evolution because of the acceptor states (I_s, V_{Zn}) in ZnS.[5d] Moreover, the extensively investigated $Zn_{1-x}Cd_xS$ with tunable parameters and lower

acceptor states than that in ZnS was selected as an interfacial layer;[15] ii) ZnS-ethylenediamine ($ZnS(en)_{0.5}$) was adopted as a template for fabricating the porous $ZnS/Zn_{1-x}Cd_xS/CdS$ heterojunction,[16] which is especially important for the water-splitting reaction because of its surface reaction characteristics;[5a, 5c, 17] iii) a post-annealing process, which has been widely employed to improve the properties of oxides but has rarely been used in sulfide heterojunctions,[16a, 18] was adopted to improve the interface state and photocatalytic activity of the sample with an interface while maintaining the heterojunction.

Herein, a $ZnS/Zn_{1-x}Cd_xS/CdS$ three-dimensional (3D) mesoporous heterostructure that exhibits a very high charge separation efficiency and H_2-evolution rate is designed and successfully fabricated for the first time. The mediating $Zn_{1-x}Cd_xS$ interface, which possesses a tunable lattice constant and band structure, acts as the charge-carrier transport channel, which favors the improvement of the charge separation efficiency. Moreover, the H_2-production rate and stability of the heterostructure involving two sulfides are dramatically improved simultaneously via the careful modification of the interface state via a simple post-annealing method. The sample prepared with the optimal parameters exhibits an excellent H_2-production rate of 106.5 mmol/h/g under visible light, which is considerably greater than that of the other previously reported CdS-based photocatalysts. Moreover, the heterostructure exhibits excellent photocatalytic stability over a period of 60 h. The well-modulated interface state is responsible for the substantially improved photocatalytic activity and stability.

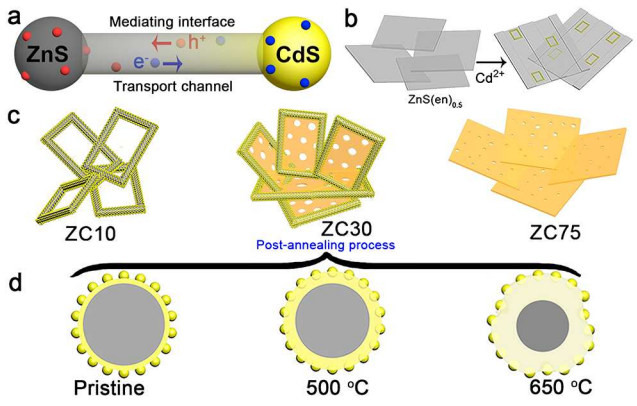

Scheme 1 (a) Scheme of the mechanism for improving charge-carrier transport in a $ZnS/Zn_{1-x}Cd_xS/CdS$ heterojunction. (b) Schematic illustrating the structural evolution of the mesoporous nanoframe derived from $ZnS(en)_{0.5}$ nanosheets. (c) Morphology of ZCX samples with different Cd^{2+} content. (d) Effect of the post-annealing process on the microstructural of ZC30.

Results and Discussion

$ZnS(en)_{0.5}$ nanosheets, which were synthetized using a modified solvothermal method,[2c] were reacted with different concentrations of Cd^{2+} at 140 °C. A series of samples with nominal Cd/Zn molar ratio x are labeled as ZCX (X = 0, 2, 6, 10, 30, 40, 75 at%). Scheme 1b shows the morphology evolution of the $ZnS/Zn_{1-x}Cd_xS/CdS$ nanoframe. The $ZnS(en)_{0.5}$ nanosheets were transformed into disorder porous ZnS with the dissolution of EDA molecules gradually (Fig. S1), which then reacted with Cd^{2+} and formed the regular rectangular nanoframe $ZnS/Zn_{1-x}Cd_xS/CdS$ heterostructure. As confirmed by the time dependence of the microstructure (Fig. S2), Cd^{2+} sculpted the $ZnS(en)_{0.5}$ nanosheets layer-by-layer and the rectangular nanoframe morphology was finally synthesized via self-assembly process (Scheme 1c and Fig. S3) because of the larger size of the $ZnS(en)_{0.5}$ nanosheets compared to the reaction-zone width.[19] As shown in Scheme 1c, the rectangular nanoframe was transformed into nanosheets with the Cd^{2+} content increasing from 10 to 75 at% (Fig. S3), with ZC30 possessing a 3D porous microstructure constructed by nanoframes connected with porous nanosheets (Figs. 1a and c). To further improve its interface state, ZC30 was post-annealed at different temperatures; the resulting samples are abbreviated as ZC30-Y (Y = 450, 500, 550, 650 °C). Scheme 1d shows the cross-section microstructural evolution of ZC30 at different post-annealing temperatures. The post-annealing process at higher temperatures may facilitate the reaction between ZnS, CdS and $Zn_{1-x}Cd_xS$ interfacial layer, and decrease the Cd^{2+} concentration in the interface solid solution and size of CdS quantum dots (CdS QDs). ZC30-500 exhibits a similar microstructure, although it is less porous compared to that of pristine ZC30 (Figs. 1b and d); in contrast, ZC30-650 presents a denser and destructed microstructure (Fig. S3f). As shown in energy-dispersive X-ray (EDX) spectrum (Fig. S4), the ratio of Cd/(Zn+Cd) in the ZC10 and ZC30 samples from EDX results is very near to the setting value, which indicates that Cd^{2+} reacted with sufficient ZnS via cation exchange reaction. However, the samples with larger Cd^{2+} content show much smaller ratio of Cd/(Zn+Cd) than the setting value, which may be attributed to the inhibited reaction between ZnS and Cd^{2+} by interfacial layer. Especially, for the heterostructure sample with Cd/Zn ratio of 150 at%, the Cd/(Zn+Cd) ratio from EDX (79.2 at%) did not increase dramatically in comparison with ZC95. Moreover, no remarkable composition variation was observed in the post-annealed samples (Fig. S5).

The X-ray diffraction (XRD) patterns of the samples with different Cd^{2+} contents (Fig. S6a) show the increasing hexagonal and cubic phases of CdS with increasing content of Cd^{2+} resulting from the limited S source.[20] However, the characteristic peak of ZnS did not disappear even in ZC75, further confirming that the interfacial solid solution inhibited complete cation exchange between ZnS and Cd^{2+}. Moreover, the peak corresponding to $Zn_{1-x}Cd_xS$ slightly shifted to lower 2-theta values with the increased Cd^{2+} content, and ZC30 exhibited a similar phase structure but with shifted peak positions compared to those of a ZnS and CdS mechanical mixture (Fig. S7), thereby indicating the formation of a $Zn_{1-x}Cd_xS$ phase. As shown in Fig. S6b, the post-annealing process dramatically improved the crystallinity in ZC30 without the formation of any extra phases. The peak corresponding to $Zn_{1-x}Cd_xS$ shifted to higher 2-theta values with increasing temperature, indicating that the content of Cd in $Zn_{1-x}Cd_xS$ decreased because of the reaction between ZnS and the interfacial layer at high temperatures. Fortunately, $ZnS/Zn_{1-x}Cd_xS/CdS$ heterostructure was well maintained even at 650 °C because of the presence of interface.

To further confirm the ZnS/$Zn_{1-x}Cd_xS$/CdS heterostructure in the as-prepared samples, element mapping and high-resolution TEM (HRTEM) were used to investigate the element distribution and phase structure of ZC30 (Figs. 1e and f). S and Zn were distributed evenly in the entire skeleton of the nanoframe, whereas Cd was primarily distributed at the edge of the nanoframe; this result was further confirmed by the smaller ratio of Cd/Zn at the center of the nanoframe (Fig. S8). As shown in Fig. 1f, the lattice fringe of the nanoregion centralized in the edge of the nanoframe can be indexed as CdS. The lattice constant of $Zn_{1-x}Cd_xS$ surrounding CdS QDs increases as the distance to the CdS nanoregion increases, and the lattice fringe of ZnS is observed far from the CdS nanoregion. This composition gradient (corresponding to different band structures) and the in-situ formation of a stably embedded interface can reduce heterostructure stress and defect concentration and hence improve the separation and transport efficiency of charge carriers.[9a, 9b] Compared with the pristine ZC30, the ZC30-500 possesses a higher crystallinity with smaller CdS QDs. Fortunately, CdS QDs can still be observed in ZC30-650 (Fig. S9), indicating the important role of the interface in maintaining the ZnS/$Zn_{1-x}Cd_xS$/CdS heterostructure.

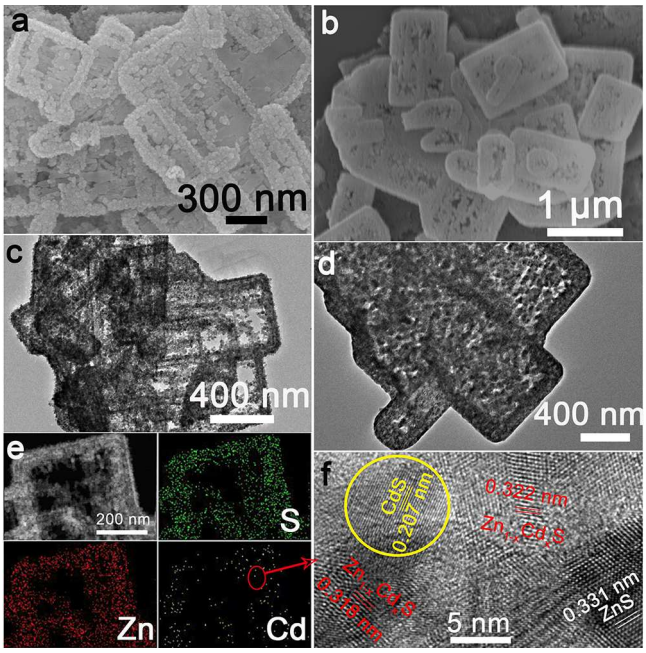

Fig. 1 Scanning electron microscopy (SEM) and transmission electron microscope (TEM) images of (a), (c) ZC30 and (b), (d) ZC30-500, respectively. (e) Element mapping and (f) HRTEM images of ZC30.

The effects of the Cd^{2+} concentration and post-annealing process on the band structure of the ZnS/$Zn_{1-x}Cd_xS$/CdS heterostructure were investigated using UV-Visible diffuse reflection spectroscopy and shown in Fig. 2a. The band edge of the heterostructure dramatically shifted to longer wavelengths in the sample with only 10 at% Cd^{2+}. All of the samples exhibited similar Eg irrespective of the Cd^{2+} loading, which is in complete contrast to the Eg values of the $Zn_{1-x}Cd_xS$ solid solution.[12a] This result may be attributed to the formation of CdS QDs resulting from the cation-exchange characteristics and the larger radius of Cd^{2+} (0.97 Å) relative to that of Zn^{2+} (0.74 Å).[14a, 21] Notably, the spectra of ZC10 and ZC30 show two band edges, and the entire diffuse reflection spectra are divided into two regions, with regions I and II corresponding to absorption in the UV and visible regions, respectively. Egs in visible and UV region are calculated by the Kubelka−Munk (KM) method (Fig. S10) and listed in inset of Fig. 2a. The Eg in region I, which represents the $Zn_{1-x}Cd_xS$ solid solution, decreased with increasing Cd^{2+} concentration, consistent with the XRD results. The Egs in region II doesn't change dramatically for the samples ranging from ZC10 to ZC75. ZC30-500 shows slightly larger Eg of CdS (2.50 eV) than that in ZC30 (2.37 eV). This can be explained by the decreased size of CdS QDs (Fig. S9a) resulting from the reaction between a little amount of CdS and the interfacial layer.[21] With further increasing temperature to 650 °C, the drastic reaction of $Zn_{1-x}Cd_xS$ as confirmed by the XRD patterns (Fig. S6) in ZC30-650 dramatically increases its band gap from 2.37 to 2.79 eV. Nitrogen and water vapor adsorption/desorption isotherms of photocatalysts with different Cd concentrations are presented in Fig. 2b. ZC30 exhibited the highest water vapor and N_2 adsorption volumes and specific surface area (S_{BET}) of 105 m^2/g (Fig. S11), which is much larger than that of other photocatalysts.[2c, 15, 22]. Fortunately, ZC30-500 exhibited relatively high S_{BET} of 43.6 m^2/g, whereas ZC30-650 shows very low S_{BET} of 14.5 m^2/g (Fig. S12).

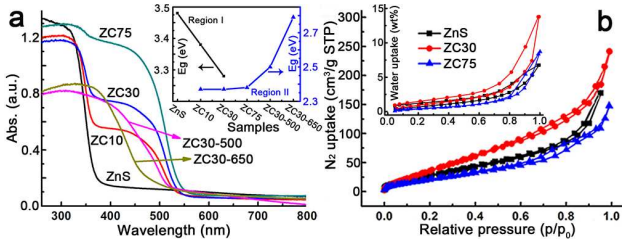

Fig. 2 (a) Effects of Cd content and the post-annealing process on the UV−visible diffuse reflection spectra and band gaps (inset) of heterostructure samples. (b) Nitrogen and water vapor (inset) adsorption/desorption isotherms of heterostructure samples.

The photocatalytic production of H_2 by ZnS/$Cd_xZn_{1-x}S$/CdS heterostructures with different Cd^{2+} contents was compared under visible-light irradiation ($\lambda \geq 420$ nm) (Fig. 3a).[2c] In contrast to the negligible visible-light hydrogen evolution activity in mesoporous ZnS, the H_2-production rate drastically increased with the content of Cd^{2+} increasing from 2 to 30 at%. Further increases of the amount of Cd led to a reduction in the H_2-production activity. ZC30 exhibited the highest H_2-evolution rate of 34.2 mmol/h/g. The interface with a suitable band structure and lattice constant in ZC30 acts as a transport channel and increases the photocatalytic activity, whereas the excess CdS may act as charge recombination centers and decrease the photocatalytic activity. Moreover, the maximum S_{BET} and water vapor adsorption of ZC30 increase the reaction sites and absorption capacity of photons and water molecules. The charge-carrier separation and transport efficiencies were further

confirmed via electrochemical impedance spectroscopy (EIS) (Fig. S13). The spectrum of ZC30 shows a smaller semicircle in the middle-frequency region compared to that of ZC75 and CdS, indicating that it possesses the fastest interfacial electron transfer arising from the well-modulated interfacial layer. To qualitatively confirm the extremely important role of interfacial layer on the H_2-procuction activity, the sulfur source (Na_2S) was added with Cd^{2+} to inhibit the formation of $Zn_{1-x}Cd_xS$ interface layer.[5d, 23] As shown in Fig. S14, both the intensity of CdS and ZnS phase get stronger with increasing the amount of sulfur source. Correspondingly, the H_2-production activity decreases dramatically because of the inhibited formation of $Zn_{1-x}Cd_xS$.

Post-annealing method, which has been extensively employed to improve the properties of oxides but has rarely been applied to sulfide heterojunctions,[16a, 19] was adopted to investigate the effects of interfacial states on the photocatalytic H_2-evolution activity of ZC30. As shown in Fig. 3b, the photocatalytic H_2-evolution activity first increased and then decreased with increasing post-annealing temperature. ZC30-500 exhibited the maximum H_2-evolution rate of 106.5 mmol/h/g, which is 152 and 966 times greater than those of CdS prepared using ethylenediamine and deionized water as the solvent, respectively (Fig. S15). In contrast, at higher temperatures, more ZnS and CdS reacted with the $Zn_{1-x}Cd_xS$ interface drastically increased the Eg and thickness of the interfacial layer, and hence, decreased the photocatalytic activity. Moreover, the deteriorated microstructure and substantially decreased S_{BET} is another explanation for the depressed H_2-evolution activity in the samples prepared at higher temperatures. The photocatalytic H_2-production activity of ZC30-500 is considerably higher than the other CdS-based photocatalysts (Table S1),[2a, 5d, 6b, 7, 16a, 24] indicating the extremely important role of the mediated interfacial state in improving the charge-separation efficiency and photocatalytic activity. The result of the comparison of the photocatalytic stabilities of the pristine ZC30 and ZC30-500 measured without renewing the sacrificial solution is presented in Fig. 3c. The pristine ZC30 exhibits a relatively good stability of 20 h because of the intimate heterojunction, efficient spatial charge separation and suitable band-structure matching.[12a] Interestingly, ZC30-500 exhibits a considerably higher H_2-production rate and longer photocatalytic lifetime over 60 h in comparison with ZC30 because of its faster interfacial electron transfer as confirmed by its much smaller semicircle in the middle-frequency region (Fig. S13). This result is attributed to the further improvement of interface state via the post-annealing process, thereby confirming the hypothesis that the improved interface state can simultaneously enhance photocatalytic activity and stability. Neither microstructure nor XRD patterns in ZC30-500 exhibited distinct variations after 60 h of photocatalytic reaction (Fig. S16), further confirming its excellent photocatalytic stability.

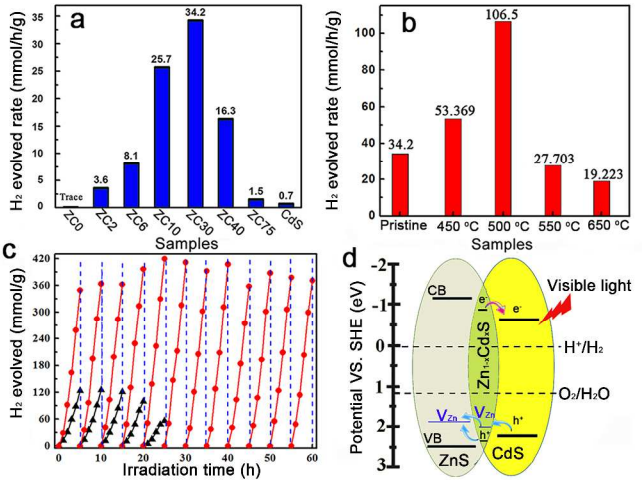

Fig. 3 (a) Photocatalytic H_2-production activities of ZCX samples and (b) ZC30 post-annealed at different temperatures in a 0.35 M Na_2S and 0.25 M Na_2SO_3 mixed aqueous solution under visible-light irradiation. (c) Comparison of the photocatalytic stabilities of pristine ZC30 (triangle) and ZC30-500 (circle). (d) Schematic illustrating charge transfer and separation in $ZnS/Zn_{1-x}Cd_xS/CdS$.

The mechanism for the separation and transport of photon-generated charge carriers in the heterostructure is shown in Fig. 3d. Photo-generated holes from the valence band (VB) of CdS transferred to the defect states of the interfacial $Zn_{1-x}Cd_xS$ layer, which then transferred into the acceptor states of ZnS because of the lower acceptor states (V_{Zn}, I_S) in $Zn_{1-x}Cd_xS$ than that in ZnS. The defect states related acceptor levels in ZnS and $Zn_{1-x}Cd_xS$ were further confirmed by the photoluminescence (PL) spectra (Fig. S17). All the heterostructure samples and the solid solution samples prepared via thermolysis method[16a] with different amount of Cd^{2+} show the similar peak position of the emission derived from different defect states (such as V_{Zn}) to that in ZnS. These results indicate the constant energy level of the defect states in ZnS, heterostructure and solid solution samples with respect to their CB edge. These results were consistent with the previous publications,[5d, 15] which reported that the peak position of the emission derived from the defect states (such as V_{Zn}) in $Zn_{1-x}Cd_xS$ is similar to that in ZnS and doesn't change with the variation of Egs derived from the different amount of Cu^{2+} dopant. Consequently, the semiconductor with lower CB edge possesses lower defect (such as I_s and V_{Zn}) related acceptor level. Meanwhile, the photo-excited electrons from the interfacial $Zn_{1-x}Cd_xS$ layer transferred to the CB of CdS QDs, which located at the outside of heterostructure. As a result, the excellent photocatalytic activity and stability in the $ZnS/Zn_{1-x}Cd_xS/CdS$ heterostructure may be a consequence of the combined effects of the following three factors: i) the mediated $Zn_{1-x}Cd_xS$ layer exhibits tunable parameters, lower acceptor states (such as V_{Zn}) than that in ZnS, which dramatically improves the matching between ZnS and CdS, and the separation efficiency of the photo-generated charge carriers; ii) the post-annealing process drastically improves the interface state and the crystallinity in the $ZnS/Zn_{1-x}Cd_xS/CdS$ heterostructure and enhances the charge separation and transport efficiency; and iii) the large S_{BET} of 105 m^2/g and interconnected 3D network in the mesoporous

heterojunction drastically increases the number of the reaction sites.

Conclusions

In summary, for the first time, we designed and successfully fabricated a ZnS/CdS 3D mesoporous heterostructure with a mediating $Zn_{1-x}Cd_xS$ interface that serves as a charge carrier transport channel. $ZnS(en)_{0.5}$ functions as both a template for the fabrication of a highly porous 3D interconnected network and as Zn and S sources for the in situ formation of a stably embedded $Zn_{1-x}Cd_xS$ interfacial layer. Furthermore, the H_2-production rate and stability of the heterostructure are simultaneously improved by the careful modification of the interface state via a simple post-annealing method. The sample prepared with the optimal parameters exhibits an excellent H_2-production rate of 106.5 mmol/h/g under visible light, which is 152 and 966 times higher than that of CdS prepared using ethylenediamine and deionized water as the solvent, respectively, and is considerable higher than that of the other CdS-based photocatalysts. Moreover, this heterostructure shows excellent photocatalytic stability over 60 h. This work not only proposed a new strategy for fabricating a water-splitting catalyst with high activity via modulating the interface state but also provide a new general route to improve the photocatalytic activity and stability of heterostructures for the effective utilization of solar energy.

Acknowledgements

This work was financially supported by NSFC (No. 21171096, 21371099, 21471081 and 21471080), the program of Jiangsu Specially-Appointed Professor, the NSF of Jiangsu Province of China (No. BK20130043 and BK20141445), the Natural Science Research of Jiangsu Higher Education Institutions of China (No. 13KJB150021), the Priority Academic Program Development of Jiangsu Higher Education Institutions, Jiangsu Planned Projects for Postdoctoral Research Funds (1302020B) and University Postgraduate Research and Innovation Project in Jiangsu Province (KYLX_0694).

Notes and references

[a] *Jiangsu Key Laboratory of Biofunctional Materials, School of Chemistry and Materials Science, Nanjing Normal University, Nanjing 210023, P. R. China. Email: yqlan@njnu.edu.cn; baojianchun@njnu.edu.cn.*

[b] *State Key Laboratory of Coordination Chemistry, School of Chemistry and Chemical Engineering, Nanjing University, Nanjing 210093, P. R. China.*

‡These authors contributed equally.

† Electronic Supplementary Information (ESI) for this article is available on DOI: 10.1039/b000000x/

1 (a) X. Zou, J. Liu, J. Su, F. Zuo, J. Chen and P. Feng, *Chem. Eur. J.,* **2013**, *19*, 2866-2873; (b) S. Li, S. Liu, S. Liu, Y. Liu, Q. Tang, Z. Shi, S. Ouyang and J. Ye, *J. Am. Chem. Soc.*, **2012**, *134*, 19716−19721; (c) X. Wang, K. Maeda, A. Thomas, K. Takanabe, G. Xin, J. M. Carlsson, K. Domen and M. Antonietti, *Nat. Mater.*, **2009**, *8*, 76-80; (d) M. Li, W. Luo, D. Cao, X. Zhao, Z. Li, T. Yu and Z. Zou, *Angew. Chem. Int. Ed.*, **2013**, *52*, 11016-11020. 1.G. Halasi, T. Bansagi, E. Varga and F. Solymosi, Catal. Lett. 2015, 145, 875; (e) Z. Yin, B. Chen, M. Bosman, X. Cao, J. Chen, B. Zheng and H. Zhang, *Small*, **2014**, *10*, 3537-3543.

2 (a) Q. Li, B. Guo, J. Yu, J. Ran, B. Zhang, H. Yan and J. R. Gong, *J. Am. Chem. Soc.*, **2011**, *133*, 10878-10884; (b) T. W. Kim and K.-S. Choi, *Science*, **2014**, *343*, 990-994; (c) J. Zhang, J. Yu, Y. Zhang, Q. Li and J. R. Gong, *Nano Lett.*, **2011**, *11*, 4774-4779; (d) J. Zhang, Q. Xu, Z. Feng, M. Li and C. Li, *Angew. Chem. Int. Ed.*, **2008**, *47*, 1766-1769.

3 A. Fujishima and K. Honda, *Nature*, **1972**, *238*, 37-38.

4 D. M. Schultz and T. P. Yoon, *Science*, **2014**, *343*, 1239176-8.

5 (a) X. Wu, Y. Yu, Y. Liu, Y. Xu, C. Liu and B. Zhang, *Angew. Chem. Int. Ed.*, **2012**, *51*, 3211-3215; (b) J. Ran, J. Zhang, J. Yu, M. Jaroniec and S. Z. Qiao, *Chem. Soc. Rev.*, **2014**, 43, 7787-7812; (c) J. Zhang, J. Yu, M. Jaroniec and J. R. Gong, *Nano Lett.*, **2012**, *12*, 4584-4589; (d) Y. P. Xie, Z. B. Yu, G. Liu, X. L. Ma and H.-M. Cheng, *Energy Environ. Sci.*, **2014**, *7*, 1895-1901.

6 (a) J. Chen, X.-J. Wu, L. Yin, B. Li, X. Hong, Z. Fan, B. Chen, C. Xue and H. Zhang, *Angew. Chem. Int. Ed.*, **2015**, *54*, 1210-1214; (b) X. Zong, H. Yan, G. Wu, G. Ma, F. Wen, L. Wang and C. Li, *J. Am. Chem. Soc.*, **2008**, *130*, 7176-7177.

7 (a) L. Huang, X. Wang, J. Yang, G. Liu, J. Han and C. Li, *J. Phys. Chem. C*, **2013**, *117*, 11584-11591; (b) J. Zhang, Y. Wang, J. Jin, J. Zhang, Z. Lin, F. Huang and J. Yu, *ACS Appl. Mater. Interfaces*, **2013**, *5*, 10317-10324; (c) Y. Tak, S. J. Hong, J. S. Lee and K. Yong, *J. Mater. Chem.*, **2009**, *19*, 5945-5951; (d) C. Xue, T. Wang, G. D. Yang, B. L. Yang and S. J. Ding, *J. Mater. Chem. A*, **2014**, *2*, 7674-7679.

8 N. Zhang, M.-Q. Yang, Z.-R. Tang and Y.-J. Xu, *ACS Nano*, **2013**. *8*, 623-633.

9 (a) P. Zhou, J. Yu and M. Jaroniec, *Adv. Mater.*, **2014**, *26*, 4920-4935; (b) C. Eley, T. Li, F. Liao, S. M. Fairclough, J. M. Smith, G. Smith and S. C. E. Tsang, *Angew. Chem. Int. Ed.*, **2014**, *53*, 7838-7842; (c) Z.-C. Zhang, B. Xu and X. Wang, *Chem. Soc. Rev.*, **2014**, *43*, 7870-7886.

10 C. Han, M.-Q. Yang, N. Zhang and Y.-J. Xu, *J. Mater. Chem. A*, **2014**, 2, 19156-15166.

11 (a) D. Chen, F. Zhao, H. Qi, M. Rutherford and X. Peng, *Chem. Mater.*, **2010**, *22*, 1437-1444; (b) J. Huang, K. L. Mulfort, P. Du and L. X. Chen, *J. Am. Chem. Soc.*, **2012**, *134*, 16472-16475.

12 (a) H. McDaniel, M. Pelton, N. Oh and M. Shim, *J. Phys. Chem. Lett.*, **2012**, *3*, 1094-1098; (b) I. Visoly-Fisher, S. R. Cohen, A. Ruzin and D. Cahen, *Adv. Mater.*, **2004**, *16*, 879-883; (c) B. Seger, A. B. Laursen, P. C. K. Vesborg, T. Pedersen, O. Hansen, S. Dahl and I. Chorkendorff, *Angew. Chem. Int. Ed.*, **2012**, *51*, 9128-9131; (d) H. Liu, J. B. Joo, M. Dahl, L. Fu, Z. Zeng and Y. Yin, *Energy Environ. Sci.*, **2015**, *8*, 286-296.

13 J. Azevedo, L. Steier, P. Dias, M. Stefik, C. T. Sousa, J. P. Araujo, A. Mendes and M. Graetzel, S. D. Tilley, *Energy Environ. Sci.*, **2014**, *7*, 4044-4052.

14 (a) B. J. Beberwyck, Y. Surendranath and A. P. Alivisatos, *J. Phys. Chem. C*, **2013**, *117*, 19759-19770; (b) D. H. Son, S. M. Hughes, Y. Yin and A. Paul Alivisatos, *Science*, **2004**, *306*, 1009-1012.

15 (a) Wllllam G. Becker and Allen J. Bard, *J. Phys. Chem.*, **1983**, *87*, 4888-4893. (b) A. K. Chawla, S. Singhal, S. Nagar, H. Om Gupta and R. Chandra, *J. Appl. Phys.*, **2010**, *108*, 123519-7.

16 (a) Q. Li, H. Meng, P. Zhou, Y. Zheng, J. Wang, J. Yu and J. Gong, *ACS Catal.*, **2013**, *3*, 882−889; (b) Y. Yu, J. Zhang, X. Wu, W. Zhao and B. Zhang, *Angew. Chem. Int. Ed.*, **2012**, *51*, 897-900.

17 (a) T. T. Zhuang, P. Yu, F. J. Fan, L. Wu, X. J. Liu and S. H. Yu, *Small*, **2014**, *10*, 1394-1402; (b) W. T. Yao, S. H. Yu, L. Pan, J. Li, Q. S. Wu, L. Zhang and H. Jiang, *Small*, **2005**, *1*, 320-325; (c) J. Zhu, Z. Yin, D. Yang, T. Sun, H. Yu, H. E. Hoster, H. H. Hng, H. Zhang and Q. Yan, *Energy Environ. Sci.*, **2013**, *6*, 987-993; (d) W. Zhou, Z. Yin, Y. Du, X. Huang, Z. Zeng, Z. Fan, H. Liu, J. Wang and H. Zhang, *Small*, **2013**, *9*, 140-147.

18 (a) W. Xi, H. Wang, X. Zeng, J. Han, J. Zhu, M. Zhou and S. Wu, *Crystengcomm*, **2014**, *16*, 6841-6847; (b) C. Cheng, A. Amini, C. Zhu, Z. Xu, H. Song and N. Wang, *Sci. Rep.*, **2014**, *4*. 4181-5.

19 S.-W. Cao, Y.-P. Yuan, J. Fang, M. M. Shahjamali, F. Y. C. Boey, J. Barber, S. C. Joachim Loo and C. Xue, *Int. J. Hydrogen Energy*, **2013**, *38*, 1258-1266.

20 (a) N. Bao, L. Shen, T. Takata, K. Domen, A. Gupta, K. Yanagisawa and C. A. Grimes, *J. Phys. Chem. C*, **2007**, *111*, 17527-17534; (b) C.

C. Nascimento, G. R. S. Andrade, E. C. Neves, C. D. A. E. S. Barbosa, L. P. Costa, L. S. Barreto and I. F. Gimenez, *J. Phys. Chem. C*, **2012**, *116*, 21992-22000.
21 J. Yu, J. Zhang and M. Jaroniec, *Green Chem.*, **2010**, *12*, 1611-1614.
22 Q. Li, H. Meng, J. G. Yu, W. Xiao, Y. Q. Zheng and J. Wang, *Chem.-Eur. J.*, **2014**, *20*, 1176-1185.
23 X. Xu, L. Hu, N. Gao , S. Liu, S. Wageh , A. A. Al-Ghamdi, A. Alshahrie and X. Fang, *Adv. Funct. Mater.*, **2015**, *25*, 445-454. (b) J. Zhang, L. Wang, X. Liu, X. Li and W. Huang, *J. Mater. Chem. A*, **2015**, *3*, 535-541.
24 Q. Wang, J. Li, Y. Bai, J. Lian, H. Huang, Z. Li, Z. Lei and W. Shangguan, *Green Chem.*, **2014**, *16*, 2728-2735.